SCIENCE CHINA
Technological Sciences

December 2011 Vol.54 Suppl. 1: 199–209
doi: 10.1007/s11431-011-4639-y

Energy analysis for damage and catastrophic failure of rocks

XIE HePing[1,2*], LI LiYun[2,1], JU Yang[2], PENG RuiDong[2] & YANG YongMing[2]

[1] *Sichuan University, Chengdu 610065, China;*
[2] *State Key Laboratory of Coal Resources and Safe Mining, Beijing Key Laboratory of Fracture and Damage Mechanics of Rock and Concrete, China University of Mining and Technology, Beijing 100083, China*

Received July 13, 2011; accepted September 23, 2011; published online November 18, 2011

The development history and current state of studies on the characteristics and mechanisms of deformation and failure of rock materials were briefly reviewed from the viewpoint of energy. The main scope and the achievable objectives of the energy-based research system were expatiated. It was validated by experiments that the damage process of rocks can be well described by the rock damage evolution equation established based on energy dissipation. It was found from the uniaxial compression and biaxial compression tests that only a small proportion of the total input energy in hard rocks is dissipated before peak load and a large proportion in soft rocks is dissipated before peak load. For both hard and soft rocks, the energy dissipated after peak load accounts for a greater proportion. More energy would be required for rock failure under equal biaxial compression than under unequal biaxial compression. The total absorbed energy is different for rock failure under high-rate loading and low-rate loading. More fragmented failure pattern usually corresponds to higher energy absorption. The mesoscopic analysis on the damage and failure of bedded salt rocks showed that the energy dissipation is prominent and the total absorbed energy for rock failure is low when cracks propagate in the weak mud interlayer while it is contrary when cracks propagate in the salt rock. The energy accumulation, transfer, dissipation and release during the failure process of tunnel with impending failure under disturbance were analyzed theoretically based on the elastoplastic mechanics theory. Furthermore, the spatial distribution of energy dissipation and energy release of fractured rocks under unloading was simulated numerically. It was demonstrated that energy is likely to be released from the weakest surface under compression, which triggers the global failure of rocks.

rock, deformation, failure, energy accumulation, energy dissipation, energy release

Citation: Xie H P, Li L Y, Ju Y, et al. Energy analysis for damage and catastrophic failure of rocks. Sci China Tech Sci, 2011, 54(Suppl. 1): 199–209, doi: 10.1007/s11431-011-4639-y

1 Introduction

The evaluation of safety and stability of underground structures relies on the proper constitutive relation, failure criteria and yield criteria of geotechnical materials and the correct calculation of stress and strain of each part of the structure. Is there any other quantitative information equivalent to stress and strain to evaluate the stability of underground structures? Studies indicated that various physical quantities related to the energy required for rock deformation and failure can be used to reflect the stress and strain of geotechnical materials or structures, for instance, acoustic emission, electromagnetic radiation, infrared radiation, temperature, and so on. Furthermore, these physical quantities can characterize the state of geotechnical materials or underground structures, which includes damage, yield, static fracturing, dynamic instability, overall structural failure, rockburst, etc. Once such corresponding relationship is identified, the current state of geotechnical materials and underground struc-

*Corresponding author (email: xiehp@scu.edu.cn)

tures might be learned directly without knowing stress or strain. In the past decades, many efforts have been dedicated to these fields and some valuable results have been achieved [1–12]. On the other hand, as catastrophic failure of underground structures received particular attention [13–16] in engineering, it has become the focus of studies on how the underground structure and the surrounding materials gradually damage, yield, fracture and fail under various excavation and construction conditions. How is the overall energy transferred and released? How much is the corresponding energy dissipated? Is the dissipated strain energy per unit volume constant or varying when the geotechnical material yields or fails under different stress conditions? Only with complete understanding of these problems, it is possible to make correct stability evaluation for underground structures. Some valuable studies have been made in these aspects by our research group and other colleagues [17–27].

1.1 Early studies

The early use of energy concept to reveal the mechanical properties of materials was proposed by von Mises in 1913, which is the distortion energy yield criterion:

$$\sqrt{\frac{1}{2}(\sigma_r-\sigma_\theta)^2+(\sigma_\theta-\sigma_z)^2+(\sigma_z-\sigma_r)^2}=k, \tag{1}$$

where k can be determined by the distortion energy obtained by uniaxial tension or compression test. Materials will yield or failure for any stress state only if the distortion energy reaches the value corresponding to uniaxial tension or compression. Therefore, this criterion is not suitable to predict the yield or failure of rock material which exhibits different properties under tension and compression.

In 1921, Griffith proposed that cracks would propagate if the released energy is larger than the propagation resistance. The tensile stress σ_{cr} for crack initiation under uniaxial tension is

$$\sigma_{cr}\approx\sqrt{\frac{2E\gamma}{\pi a}}. \tag{2}$$

In 1957, Irwin and Orwan further developed Griffith's theory and modified the crack propagation resistance. The modified tensile stress σ_{cr} for crack initiation under uniaxial tension is

$$\sigma_{cr}\approx\sqrt{\frac{E(2\gamma+\gamma_p)}{\pi a}}, \tag{3}$$

where γ and γ_p are the surface energy consumed for crack propagation by a unit area and the plastic energy in the corresponding area, respectively, $2a$ is the length of the center crack.

In 1972, Xue Changming suggested a criterion based on a minimum strain energy intensity factor. It is considered that cracks are most likely to propagate along the direction of the minimum strain energy intensity.

Hereinbefore some earlier theories related to energy and failure were reviewed. As for the rock mechanical testing techniques related to energy, the Kaiser effect of acoustic emission and the positioning technique by acoustic emission are well-known and established.

The earlier studies on theories and experiments were unmeditated and scattered. Due to the lack of systemic studies, such studies received little attention.

1.2 Recent studies

The recent studies by measuring acoustic emission signals, infrared signal, electromagnetic signal and temperature were focused on the relationship between the changes of radiation intensity or temperature and the variations of stress and strain. Some consistent conclusions are made: Rock fracturing is generally accompanied by strong acoustic emission; the strain increase is accompanied by decreasing infrared radiation intensity, electromagnetic radiation intensity and temperature after fracturing; before rock fracturing under compression, acoustic emission signal is weak while the infrared radiation intensity, electromagnetic radiation intensity and temperature would rise [1–12]. Some experimental studies [17] have shown that the change of material temperature or infrared radiation intensity is related to the volumetric strain. When the volumetric strain be- comes smaller, the temperature or infrared radiation intensity usually increases. On the contrary, when the volumetric strain increases, the temperature or infrared radiation intensity decreases. According to the thermodynamic theorem, the relationship between the temperature and the volumetric strain obeys:

$$T=\frac{k}{(1-\theta)^{\beta-1}V_0^{\beta-1}}, \tag{4}$$

where T is the temperature, θ is the volumetric strain (compression is positive), V_0 is the initial volume, k and β are material parameters. It can be seen from the above equation that the temperature T would rise with the increase of the volumetric strain θ.

Recent studies have focused on the experimental measurement of physical quantities. On the other hand, they also focused on the theoretical analyses and experimental researches, including the relationship between the amount of energy dissipation and the damage variable, the relationship between the amount of energy release and the failure process and energy-based criteria for rock failure [18–20] in order to calculate the least energy required for the rock failure under various stress conditions. These criteria can be used to estimate the energy dissipation. It was commonly recognized from theoretical analyses and experimental researches that the energy absorbed or dissipated for static

failure of rock is not constant, however, it can be expressed by mathematical formulas. The energy absorbed or dissipated for rock failure depends greatly on the stress state. More energy would be dissipated for the failure under uniaxial compression than under uniaxial tension, and even more energy would be dissipated for rock failure under confined compression [18–27].

2 Energy characteristics of rock failure under uniaxial compression

Rock failure is caused by the abrupt energy release，which is the catastrophe of energy dissipation under a certain condition. From the viewpoint of mechanics, rock deformation and failure process is a process from local energy dissipation to local failure and eventually to the global catastrophic failure. From the viewpoint of thermodynamics, the process is an irreversible process of energy dissipation and energy release. During this process, the total work of external load results in the increase of elastic strain energy in rock. In addition, part of the work is dissipated and leads to the irreversible damage of rock. The existing mechanics theories emphasize the energy dissipation and local failure process. However, the global catastrophic failure of rock is essentially the process of energy dissipation and energy release. Therefore, it is necessary to conduct further theoretical and experimental studies and establish a rock mechanics system based on analysis of energy dissipation and energy release and put it into practice to solve more problems in rock engineering.

2.1 Damage evolution of rock based on energy dissipation

Based on the analysis of energy dissipation, a rock damage evolution equation can be established and the corresponding parameters can be determined by experiments. A rock damage evolution equation was proposed by Xie et al. [19] in the following form:

$$D = 1 - \exp\left[-B\left| Y - Y_0 \right|^{\frac{1}{n}} \right]. \tag{5}$$

where B, n, Y_0 are material constants of rock depending on the properties of rock material. The relationship between the damage energy dissipation rate Y and the elastic strain energy U_e is represented by

$$Y = \frac{U_e}{1 - D}. \tag{6}$$

Because the change of elastic modulus can reflect the evolution of damage, the damage variable D can be calculated according to the unloading elastic modulus obtained by the cyclic loading and unloading test:

$$D = 1 - \frac{E}{E_0}. \tag{7}$$

Experimental results and theoretical analyses [19, 21, 22] show that the above damage evolution equation based on the analysis of energy dissipation can well describe the damage evolution of rock.

It was shown in uniaxial compression tests that most hard rocks dissipate a relatively small amount of energy before fracturing and a larger amount of energy during the failure process after peak load (see Figures 1 and 2) accompanied by intensive acoustic emission and temperature decrease (see Figure 3) [27].

2.2 Absorbed energy and releasable strain energy for rock failure

A series of tests were conducted on the same type of rock to investigate the energy dissipated during the failure process under uniaxial compression with different loading rates. Under the conventional quasi-static compression tests, no apparent correlation between the absorbed energy and the loading rate can be identified. However, the correlation is evident for rock under impact load or cyclic loading and unloading. The absorbed energy is greatly related to the

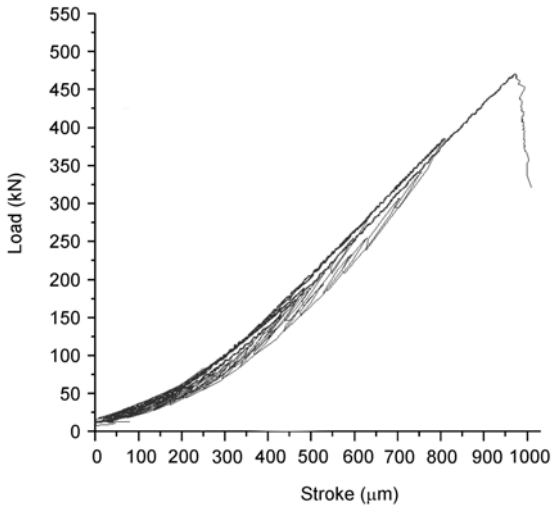

Figure 1 Small amount of energy dissipated before peak load.

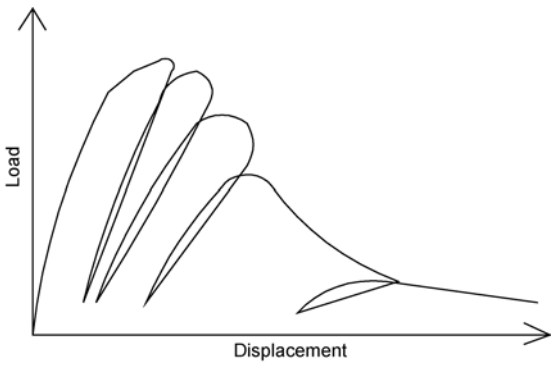

Figure 2 A sketch of large amount of energy dissipated after peak load.

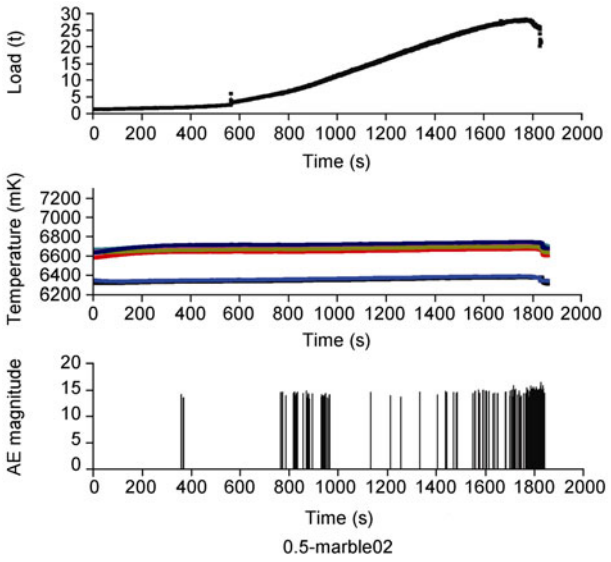

Figure 3 Variation of load, temperature and acoustic emission with time for rock under uniaxial compression.

loading rate. The absorbed energy for impact loading is obviously lower than that for static loading, and the absorbed energy for cyclic loading and unloading is apparently higher than that for continuous static loading (see Table 1). Such a relationship between the loading rate and the absorbed energy should be paid attention in engineering practices.

According to the block size analysis on fragments for rock failed under uniaxial compression, no evident correlation between the compressive strength and the failure pattern can be identified. Even for rocks with the same ultimate stress and strain, the failure pattern may be different. However, a certain relationship can be found between the degree of fragmentation and the energy absorbed by unit volume of rock. The more energy absorbed by unit volume of rock, the higher degree of fragmentation. Thus, the deformation and failure of rock can be better described from the viewpoint of energy.

The releasable strain energy in rock can be expressed as [18, 19]

$$U^e = \frac{1}{2}\sigma_1\varepsilon_1^e + \frac{1}{2}\sigma_2\varepsilon_2^e + \frac{1}{2}\sigma_3\varepsilon_3^e, \tag{8}$$

$$\varepsilon_i^e = \frac{1}{E_i}[\sigma_i - \nu_i(\sigma_j + \sigma_k)]. \tag{9}$$

Table 1 Total specific absorbed energy of granite under uniaxial compression

Loading rate	Loading mode	Total specific absorbed energy u (J/cm^3)
High	SHPB impact	0.18
Quasi-high	continuous loading	0.23
Quasi-high	repetitive loading and unloading	0.39
Moderate	continuous loading	0.30
Moderate	repetitive loading and unloading	0.52
Low	continuous loading	0.23
Low	repetitive loading and unloading	0.39

The above equations show that the releasable strain energy in rock elements depends only on the stress state σ_i, the unloading modulus E_i and Poisson's ratio ν_i, regardless of linear or nonlinear constitutive relation of rock. It was indicated by a series of uniaxial compression tests that the unloading modulus E_i and Poisson's ratio ν_i are closely related to the stress state [18]. For the convenience of engineering applications or in the case of low requirement on precision, the average releasable strain energy can be used.

3 Energy characteristics of rock failure under biaxial compression

Previous studies have focused on the energy properties of rocks under uniaxial compression. However, the stress acting on underground structures is mostly two-dimensional or three-dimensional. Therefore, biaxial compression tests should be conducted to investigate the releasable strain energy and the dissipated energy in rock under two-dimensional stress state.

The equipment of biaxial compression test is shown in Figure 4. The material under test is white marble. Two types of tests were conducted, namely, the biaxial compression test with fixed lateral displacement and the biaxial compression test with synchronous loading.

3.1 Biaxial compression test with fixed lateral displacement

As a preliminary study, six biaxial compression tests were conducted with different lateral displacements, which corresponded to six different lateral compression forces 0, 5, 10, 15, 20, and 25 kN, respectively. Figure 5 shows the variations of biaxial load with time. The force fluctuating around the horizontal line is the lateral force, and the vertical force is applied as a cyclic loading and unloading force with a loading rate of 0.1 mm/min until failure of samples (see Figure 6). The releasable strain energy, the dissipated

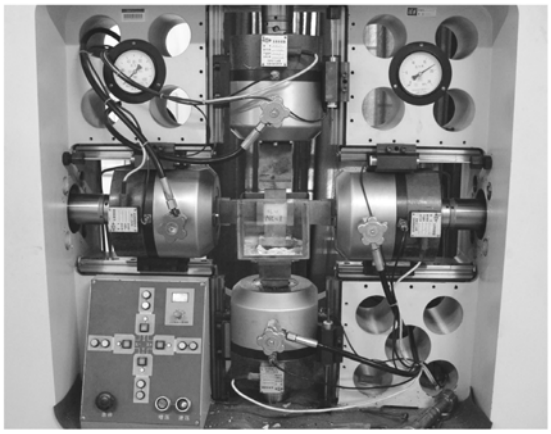

Figure 4 Biaxial compression test on marble.

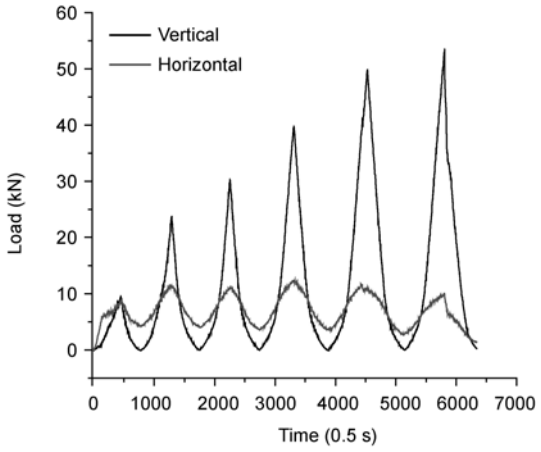

Figure 5 Variations of load in two directions with time.

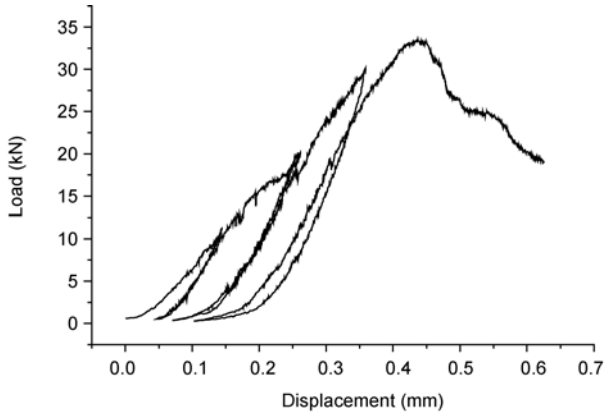

Figure 6 Vertical loading and unloading curves.

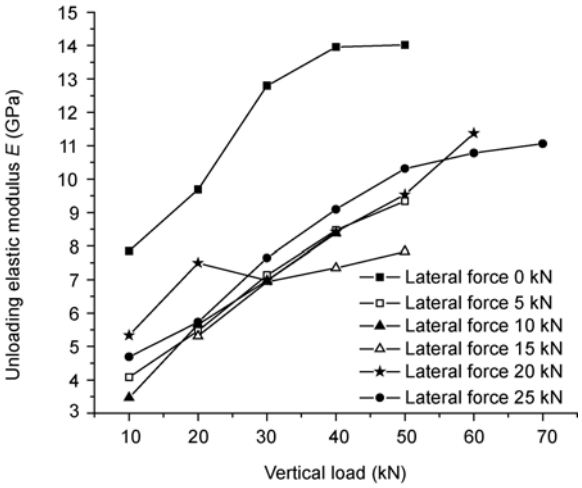

Figure 7 Unloading elastic moduli of marble under different lateral pressures.

Table 2 Total specific absorbed energy of marble under different lateral pressures

Lateral pressure (kN)	Total specific absorbed energy u (J/cm^3)
0	0.09
5	0.11
10	0.10
15	0.17
20	0.16
25	0.18

energy and the total absorbed energy can be extracted from the curves. Once the vertical load reaches the preset level, the force is unloaded to zero so as to obtain the releasable strain energy, the dissipated energy and the unloading elastic modulus under different stress states. It shall be noted that the energy stored in the testing machine shall be taken out for calculation.

If the displacement in one direction is restricted (i.e. no energy input in this direction), the loading or unloading elastic modulus along the direction perpendicular to the restricted displacement would decrease, as shown in Figure 7. The unloading elastic moduli with lateral constraint are significantly lower than those without lateral constraint. The energy absorption capacity is larger with lateral constraint than that without lateral constraint even under the same stress conditions. Attention shall be paid to this feature as it may correspond to some actual engineering conditions.

It can be seen from Figure 7 that the variation of the unloading elastic modulus is not evident with the increasing of the lateral force excepte the 0 kN lateral force situation.

The experimental results also show that the greater the average lateral displacement or lateral pressure, the more work or energy is required for rock fracturing. The experimental results are listed in Table 2.

3.2 Biaxial compression test with synchronous loading

Four biaxial compression tests with synchronous loading and unloading were conducted with loading rates of 0.1, 0.15, 0.2, and 0.25 mm/min, respectively. The aims of the tests were to investigate the effect of loading rate on the unloading elastic modulus, the releasable strain energy and the dissipated energy. Figure 8 shows the curves of load in the x and y directions versus time, and Figures 9 and 10 show the variations of displacement with cyclic loading and unloading along the x and y direction, respectively.

As can be seen from Figures 6, 9 and 10, a relatively large amount of energy is dissipated before the peak load due to loose internal structure and low modulus of low-strength white marble. It is totally different compared to the hard rock with compacted structure, high compressive strength and elastic modulus, as shown in Figure 1. For the white marble, the dissipated energy is about 50% of the total input energy in each loading cycle, and sometimes reaches 60%. Thus, the dissipated energy is almost equal to the releasable strain energy. It means that for soft rocks the dissipated energy accounts for a higher proportion while the capacity of releasable strain energy is lower.

Table 3 shows that the total specific absorbed energy has no apparent correlation with the loading rate for rock samples under the same load. However, by comparing Tables 2

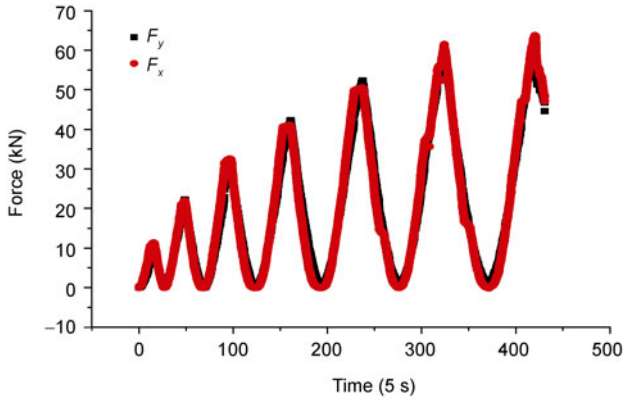

Figure 8 Variations of biaxial forces F_x and F_y with time.

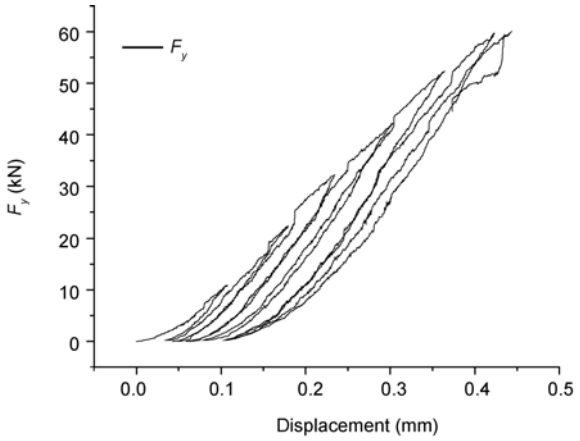

Figure 9 The loading and unloading curves of vertical force F_y.

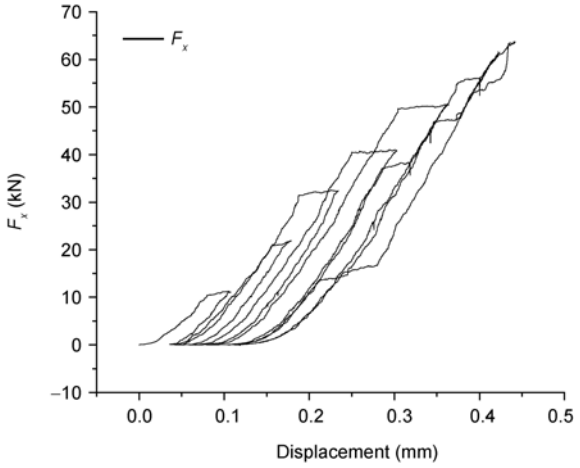

Figure 10 The loading and unloading curves of horizontal force F_x.

Table 3 Total specific absorbed energies of marble under synchronous biaxial loading

Peak load (kN)	Total specific absorbed energy (J/cm^3)			
	Loading rate (mm/min)			
	0.1	0.15	0.2	0.25
80	1.78	2.04	1.78	1.72
90	2.26	2.76	2.44	------

and 3, it can be seen that the total specific absorbed energy of the white marble which failed under biaxial compression with synchronous loading is obviously larger than that under biaxial compression with small lateral pressure.

4 Mesoscopic mechanism of rock damage and failure

The essence of rock damage evolution is the irreversible degradation of the internal microscopic and mesoscopic structures, which also can manifest the changes of rock properties. By using a servo testing system with a scanning electron microscope, tensile tests were conducted on rock samples. Real-time SEM images were captured for rock surfaces during the deformation and failure process to investigate the damage evolution process. Experimental results show that the surface morphology changes irreversibly until the final macroscopic tensile cracks appear [21, 22]. The SEM images were processed by threshold segmentation, edge detection and other image processing methods. The fractal dimension of SEM images was calculated and selected as the parameters for description of the mesoscopic morphology of rock surfaces. It was found that the increase of load leads to larger fractal dimension of rock surfaces and more severe damage in rock.

Mesoscopic experiments revealed the energy dissipation in rocks under loading and the resulted irreversible damage evolution. In order to further study the law of energy release upon rock failure, real-time evolution of cracks in bedded salt rock samples was investigated by means of the testing system with SEM. The mesoscopic failure mechanism was discussed based on the energy analysis. It was indicated by experimental observations that great difference exists between the meso-structures of salt rock and mud interlayer, which affects the macroscopic mechanical behavior of bedded salt rock.

Figure 11 shows the histogram of the peak load, the maximum deflection and the work of external loads for each sample. It was found by comparison that cracks would propagate in salt rock if the work of external load is large and thus the strength of the samples is high, while cracks would propagate in the mud interlayer if the work of external load is small and thus the strength of the samples is low. Therefore, the crack propagation in rock can be better explained from the viewpoint of energy. Generally, cracks propagate in salt rock or the mud interlayer instead of along the interface of salt rock and the mud interlayer. When cracks propagate in the mud interlayer, energy dissipation plays an important role so that the path of cracks is irregular and cracks even branch out sometimes. In this case, the load-bearing capacity of bedded salt rock is low, and eventually a small amount of work by external force would result in failure of salt rock (see Figure 12(a)). When cracks propagate the salt rock, more elastic energy is released

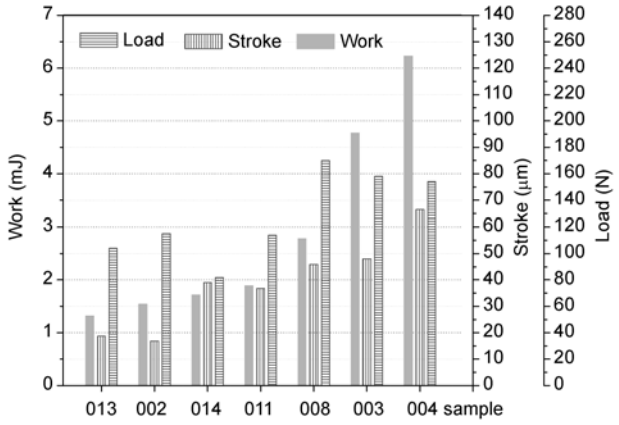

Figure 11 Histogram of peak load, maximum deflection and work by external load.

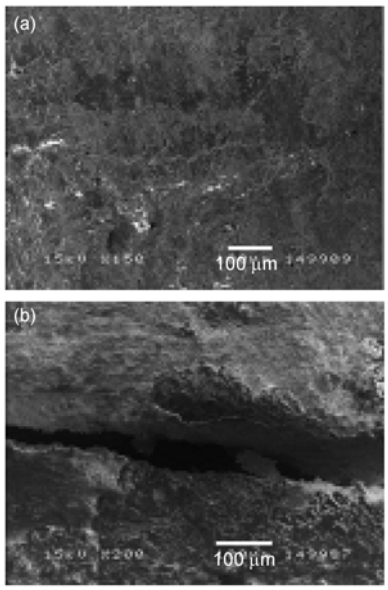

Figure 12 SEM images of cracks in salt rock and mud interlayer. (a) Crack propagation in mud; (b) crack propagation in salt rock.

rapidly so that the path of cracks is straight and cracks even open up sometimes. In this case, the load-bearing capacity of bedded salt rock is higher and subsequently more work by external work would be absorbed (see Figure 12(b)).

5 Theoretical analysis on energy transfer and release in tunnel

The characteristics of energy release and dissipation have been discussed for a variety of rocks under uniaxial compression and biaxial compression. The characteristics of energy release and dissipation under triaxial compression need further experimental exploration. In short, given the constitutive relation, the average unloading elastic modulus and Poisson's ratio, the stress distribution and energy-based failure criteria, the dissipated energy and releasable energy during the failure process can be calculated. The energy release process after failure can be estimated. In the next section, the energy release process is analyzed theoretically based on failure of an underground mining tunnel due to disturbance.

Figure 13 shows a horizontal tunnel in a sufficiently large geo-mass. For convenience of analysis, the geo-stress around tunnel is constant and has a value of q. If the horizontal stress and the vertical stress are not equal, the analysis process can be implemented using numerical simulation. Assume the constitutive relation of rock under uniaxial compression is as follows:

$$\sigma = A\varepsilon^m, \tag{10}$$

where A and m are material parameters. As shown in Figure 14, m<1, m=1 and m>1 correspond to the convex non-linear, linear and concave nonlinear constitutive relation, respectively. The constitutive relations of all sorts of geo-materials can be approximately expressed by eq. (10) with different values of A and m.

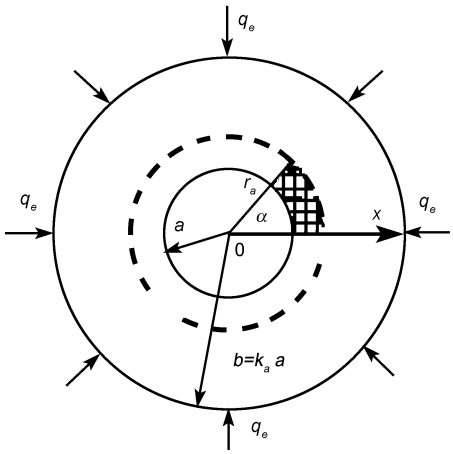

Figure 13 Tunnel with radius a in a sufficiently large geo-mass ($k_a \geqslant 10$).

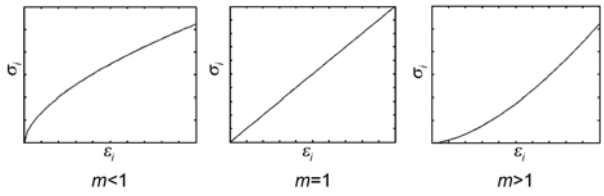

Figure 14 The constitutive relation of rock under uniaxial compression.

The tunnel shown in Figure 13 is under hydrostatic pressure q_e. If the excavated diameter a is large, the tunnel is in an impending failure state. Considering a disturbance stress increment Δq a certain distance, as the tunnel is not supported, collapse or rockburst may occur. Now the dissipated energy, the releasable energy and the ejected velocity of

rock blocks by rockburst (intensity of rockburst) could be estimated.

According to the plastic mechanics theory [28], the constitutive relation equation shown in eq. (10) can be applied to rocks under complex stress state to represent the relationship between stress intensity and strain intensity.

$$\sigma_i = \phi(\varepsilon_i) = A\varepsilon_i^m. \tag{11}$$

In cylindrical coordinates, the stress intensity can be expressed as

$$\sigma_i = \frac{\sqrt{2}}{2}\sqrt{(\sigma_r-\sigma_\theta)^2+(\sigma_\theta-\sigma_z)^2+(\sigma_z-\sigma_r)^2}. \tag{12}$$

The strain intensity can be expressed as

$$\varepsilon_i = \frac{\sqrt{2}}{3}\sqrt{(\varepsilon_r-\varepsilon_\theta)^2+(\varepsilon_\theta-\varepsilon_z)^2+(\varepsilon_z-\varepsilon_r)^2}. \tag{13}$$

According to the total strain theory in plastic mechanics, the stress components can be obtained by applying the equilibrium equation, geometric equation, constitutive relation and stress boundary condition to the axial symmetrical plane strain problem shown in Figure 13, i.e.,

$$\begin{cases} \sigma_r = \sigma_3 = q_e\left(1-\dfrac{a^{2m}}{r^{2m}}\right)K_a, \\ \sigma_\theta = \sigma_1 = q_e\left[1+\dfrac{(2m-1)a^{2m}}{r^{2m}}\right]K_a, \\ \sigma_z = \sigma_2 = q_e\left[1+\dfrac{(m-1)a^{2m}}{r^{2m}}\right]K_a, \end{cases} \tag{14}$$

$$\begin{aligned} K_a &= \frac{k_a^{2m}}{k_a^{2m}-1}, \\ K_a &= \frac{b}{a}, \end{aligned} \tag{15}$$

where the compressive stress is positive, and each component is independent of A.

According to eq. (14), it can be verified by various failure criteria that failure will first occur in the inner tunnel wall shown in Figure 13.

By applying the energy-based failure criterion proposed by Xie et al. [18]:

$$\begin{aligned} &(\sigma_1-\sigma_3)[\sigma_1^{\,2}+\sigma_2^{\,2}+\sigma_3^{\,2} \\ &-2\mu(\sigma_1\sigma_2+\sigma_2\sigma_3+\sigma_3\sigma_1)] = \sigma_c^3, \end{aligned} \tag{16}$$

the relationship of the ultimate geo-stress q_e, with the tunnel radius a and the compressive strength σ_c can be obtained as

$$q_e = \frac{1}{mK_a\sqrt[3]{10-8\mu}}\sigma_c. \tag{17}$$

By applying the Mises energy-based yield criterion characterized by compressive strength:

$$\sigma_i = \sqrt{\frac{1}{2}(\sigma_r-\sigma_\theta)^2+(\sigma_\theta-\sigma_z)^2+(\sigma_z-\sigma_r)^2} = \sigma_c, \tag{18}$$

the relationship of the ultimate geo-stress q_e with the tunnel radius a and the compressive strength σ_c can be obtained from eq. (18) as

$$q_e = \frac{1}{K_a.\sqrt{3}m}\sigma_c. \tag{19}$$

Table 4 lists ultimate geo-stresses q_e values based on various failure criteria. The following parameters are adopted for calculation: m=0.8, compressive strength σ_c = 40.58 MPa, tensile strength σ_t = 4 MPa, unloading Poisson's ratio μ=0.26 and internal friction angle ϕ=30°. These mechanical parameters are basically consistent with those of the aforementioned white marble.

The underground tunnel shown in Figure 13 is in the critical failure state under the geo-stress q_e listed in Table 4. If a positive stress increment Δq is adopted in the surrounding geo-mass, the damage in the inner tunnel wall will further develop radially to the position with a radius of r_s (see Figure 13). The failure depth h_s is

$$h_s = r_s - a. \tag{20}$$

A different failure radius r_s and failure depth h_s are obtained if a different failure criterion is adopted. The failure radius r_s determined by eq. (16) can be given by the following equation:

$$\begin{aligned} &2mK_a^3\left(q_e+\Delta q\right)^3\frac{a^{2m}}{r_s^{2m}}\left\{3(1-2\mu)+6(1-2\mu)(m-1)\frac{a^{2m}}{r_s^{2m}}\right. \\ &\left.+[(5-4\mu)m^2+3(1-2\mu)(1-2m)]\frac{a^{4m}}{r_s^{4m}}\right\} = \sigma_c^3. \end{aligned} \tag{21}$$

The failure radius r_s can be obtained from the Mises criterion (eq. (18)) in the following form:

$$r_s = a\sqrt[2m]{\frac{\sqrt{3}mK_a(q_e+\Delta q)}{\sigma_c}}. \tag{22}$$

Table 4 Values for the ultimate geo-stress q_e obtained by various failure criteria

Criterion	Tresca	Coulomb-mohr	Xie et al. [18]	Mises	Double shear [29]
q_e (MPa)	25.085	25.085	25.169	28.97	33.45

If $\Delta q = 0.3q_e$, the failure depth h_s is approximately $0.3a$, if calculated by eqs. (20) and (21) and the aforementioned mechanical parameters. The failure depth h_s is about $0.2a$ if calculated by eqs. (20) and (22).

With known failure depth h_s, the surrounding geo-mass within the depth is considered to be failed due to yield or broken. The releasable strain energy stored in the surrounding geo-mass is exhausted by various activities, such as development of new fracture surfaces, sound, heat, electromagnetic radiation, etc. If the region covered by the angle α shown in Figure 13 is the region with weak geological structure, the rock material in this region would be ejected. The energy is provided by the whole underground structure, i.e., the releasable strain energy of the whole structure, which can be expressed as

$$U_e = U_{1e} - U_{2e}. \tag{23}$$

U_e is the difference between the releasable strain energy in the two structures shown in Figure 15 and can be calculated. In Figure 15, $q_m = q_e + \Delta q$.

U_{1e} is the strain energy in the intact region when the stress q_{rs} exists at the interface of the damaged region and the intact region. q_{rs} can be calculated by eq. (14). U_{2e} is the strain energy in the intact region during rockburst and zero stress is assumed on the tunnel inner wall.

q_d in Figure 15(b) is the attenuated geo-stress after rockburst at a certain distance. Let the displacement on the external wall of tunnel be fixed during the energy release process from Figure 15(a) to 15(b), in another word, no more work by external forces is applied to the structure in this process. According to the displacement compatibility on the external wall, the relationship between q_d and q_m can be obtained by the plastic mechanics theory.

$$\begin{aligned} q_d &= \frac{a^{2m}}{r_s^{2m}} q_m = \frac{q_m}{k_s^{2m}}, \\ k_s &= \frac{r_s}{a} \end{aligned} \tag{24}$$

The strain energies per unit thickness U_{1e} and U_{2e} can be calculated by integrating the intensity factors of strain energies u_{1e} and u_{2e} along the ring. The intensity factor of strain energy can be expressed as

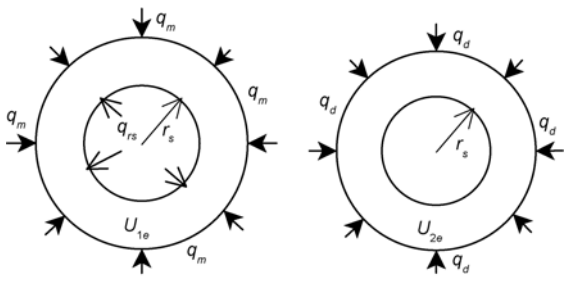

Figure 15 The mechanical meaning of releasable strain energies U_{1e} and U_{2e}.

$$u_{ie} = \frac{1}{2E}[\sigma_1^2 + \sigma_2^2 + \sigma_3^2 - 2\mu(\sigma_1\sigma_2 + \sigma_2\sigma_3 + \sigma_3\sigma_1)], \tag{25}$$

where E and μ are the mean values of unloading elastic modulus and Poisson's ratio, respectively.

Following the idea presented above, we have

$$\begin{aligned} U_e &= U_{1e} - U_{2e} = \int_0^{2\pi}\int_{r_s}^{b} (u_{1e} - u_{2e}) r \mathrm{d}\theta \mathrm{d}r = \\ &= \int_0^{2\pi}\int_{k_s.a}^{k_a.a} (u_{1e} - u_{2e}) r \mathrm{d}\theta \mathrm{d}r = \\ &= \frac{3q_m^2 a^2 \pi K_a^2}{2E}(1-2\mu)\left[\begin{array}{l}\left(1-\frac{1}{k_s^{4m}}\right)(k_a^2 - k_s^2) + \\ +2\left(1-\frac{1}{k_s^{2m}}\right)\left(\frac{1}{k_a^{2m-2}} - \frac{1}{k_s^{2m-2}}\right)\end{array}\right]. \end{aligned} \tag{26}$$

If all the strain energy is provided to the free rock fragments within the shaded area covered by the angle α, then the ejection velocity can be obtained as

$$v_\alpha = \sqrt{\frac{4U_e}{(r_s^2 - a^2)\alpha\rho}}. \tag{27}$$

6 Numerical simulation of failure energy for fractured rock

The finite element method was adopted to simulate the triaxial loading-unloading test on fractured coal with calcite inclusion and to investigate the characteristics of energy release and accumulation in the deformation process. The numerical model is a 50 mm×50 mm×50 mm cube. The confining pressure of 10 MPa is imposed in the x and z directions and an axial stress of 20 MPa along the y direction is applied on the model surfaces. Two unloading paths were simulated, namely, unloading only on one side in the x direction, and unloading on both sides in the x direction. The simulation results are shown in Figure 16.

It can be seen from Figure 16 that the energy in failed coal elements is almost uniform before unloading, except some elements with high energy appearing near the internal cracks of coal. For the case of unloading on one side, the increase of the unloaded confining pressure results in more failed elements near the unloaded surface. A great amount of high-energy failed elements appear and eventually severe damage occurs on the unloaded surface. For the case of unloading on both sides, some symmetrically distributed failed elements appear near both unloaded surfaces. These elements are within the high-energy zone. With gradual increase of unloaded confining pressure, the number of failed elements increases and eventually severe damage occurs symmetrically on unloaded faces.

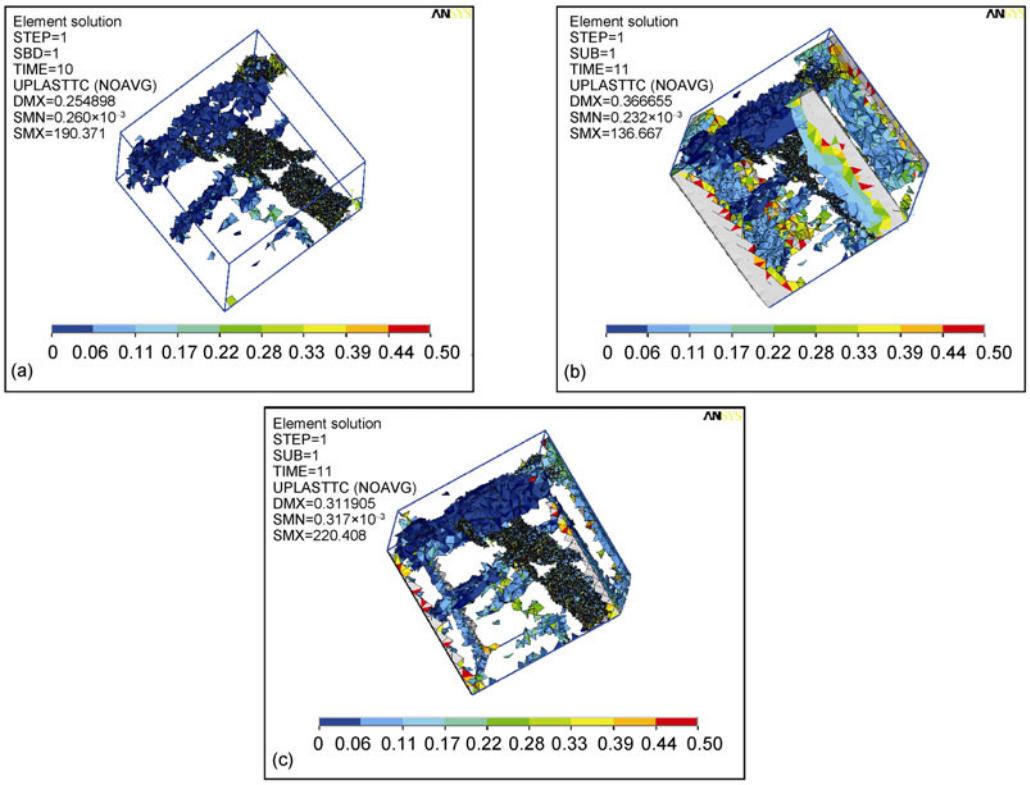

Figure 16 The energy distribution of failed coal elements under loading and unloading. (a) Loading (axial pressure 20 MPa, confining pressure 10 MPa); (b) unloading only on one side (axial pressure 20 MPa, confining pressure 0 MPa); (c) unloading on both sides (axial pressure 20 MPa, confining pressure 10 MPa).

7 Conclusions

(1) The development history of studies on material deformation and failure was briefly reviewed from the viewpoint of energy. It is indicated that the scope and depth of the energy-based research system can be further explored.

(2) The state of the art of researches on the relationship of energy with deformation and failure of rocks was introduced. Then the scope and achievable objectives were explained.

(3) It is verified by a large amount of experiments that the rock damage evolution equation based on energy dissipation can well describe the damage evolution of rocks. The evolution equation indicates the one-to-one correspondence between energy dissipation and damage.

(4) It was found from the uniaxial compression and biaxial compression tests that only a small proportion of the total input energy is dissipated before the peak load for hard rocks, while a larger proportion is dissipated by soft rocks. A large proportion of the total energy is dissipated after the peak load for both hard and soft rocks. Experimental results are helpful in estimating the energy dissipation during the failure process of rock structures. More energy would be required for rock failure under biaxial equal compression than that under biaxial unequal compression. The results are in accordance with the prediction of energy-based criterion suggested by our research team previously.

(5) The total absorbed energy for rock failure is closely related to the loading rate. High loading rate leads to higher stress and smaller deformation, while low loading rate corresponds to smaller stress and larger deformation. The total absorbed energy under high loading rate is sometimes less than that for low loading rate. More energy is absorbed for rocks failed with more fragments.

(6) The mesoscopic study on bedded salt rock indicates that the energy dissipation is significant and that less energy is absorbed when cracks propagate in soft mud interlayer while it is opposite when cracks propagate in salt rock.

(7) Based on the elasto-plastic mechanics theory, the theoretical analysis method for energy transfer, dissipation and release during the damage process of a disturbed tunnel in the critical failure state was presented. The overall structural effect of the calculated releasable strain energy was illustrated. The releasable strain energy is closely related to the degree of catastrophic failure.

(8) The energy characteristics of fractured coal under unloading were numerically simulated. The results showed that the energy tends to be released through the unloaded surface where failure appeared. The results are well consistent with the results predicted by energy-based criteria proposed by our research group.

This work was supported by the National Key Basic Research Program ("973" Program) (Grant Nos. 2011CB201201 and 2010CB226804), the National Natural Science Foundation of Yalong River Hydropower Development Joint Research Foundation of China (Grant No. 50639100), and the National Natural Science Foundation of China (Grant Nos. 50974125 and 5112507).

1 Zheng Z S. Energy transformation during rock deformation and dynamic analysis of rock deformation. Sci China Ser B-Chem, 1991, 34(1): 104–117
2 Ju Y, Wang H J, Yang Y M, et al. Numerical simulation of mechanisms of deformation, failure and energy dissipation in porous rock media subjected to wave stresses. Sci China Tech Sci, 2010, 53: 1098–1113
3 Fukui K, Okubo S, Terashima T. Electromagnetic radiation from rock during uniaxial compression testing: The effects of rock characteristics and test conditions. Rock Mech Rock Eng, 2005, 38(5): 411–423
4 Nardi A, Caputo M. Monitoring the mechanical stress of rocks through the electromagnetic emission produced by fracturing. Int J Rock Mech Min, 2009, 46(5): 940–945
5 Tuncay E, Ulusay R. Relation between Kaiser effect levels and pre-stresses applied in the laboratory. Int J Rock Mech Min, 2008, 45(4): 524–537
6 Frid V. Rockburst hazard forecast by electromagnetic radiation excited by rock fracture. Rock Mech Rock Eng, 1997, 30(4): 229–236
7 Holtzman B, Kohlstedt D, Morgan J. Viscous energy dissipation and strain partitioning in partially molten rocks. J Petrol, 2005, 46(12): 2569–2592
8 Ju Y, Yang Y M, Song Z D, et al. A Statistical model for porous structure of rocks. Sci China Ser E-Tech Sci, 2008, 51: 2031–2039
9 Wu L X, Tand C A, Zhong S, et al. Comparison of thermal infrared radiation from discontinuous jointed faults fracturing with its acoustic emission and stress field (in Chinese). Chin J Rock Mech Eng, 2006, 25(6): 1111–1117
10 Deng M D, Qian J D, Yin J Y, et al. Research on the application of infrared remote sensing in the stability monitoring and unstability prediction of large concrete engineering (in Chinese). Chin J Rock Mech Eng, 2001, 20(2): 147–150
11 Wang E Y, He X Q, Liu Z T. The research progress of coal EMR characteristics and its application (in Chinese). Prog Nat Sci, 2006, 16(5): 532–536
12 Zhao X D, Li Y H, Yuan R F, et al. Study on crack dynamic propagation process of rock samples based on acoustic emission location (in Chinese). Chin J Rock Mech Eng, 2007, 26(005): 944–950
13 Chen, S Y, Ma J, Liu L Q, et al. Phenomenon of thermal infrared radiation before Pakistan Earthquake (in Chinese). Prog Nat Sci, 2006, 16(11): 1487–1490
14 Sanchidrián J, Segarra P, López L. Energy components in rock blasting. Int J Rock Mech Min, 2007, 44(1): 130–147
15 He M C, Miao J L, Feng J L. Rock burst process of limestone and its acoustic emission characteristics under true triaxial unloading conditions. Int J Rock Mech Min, 2009, 47(2): 286–298
16 Hamdi E, Romdhane N B, Mouza J, et al. Fragmentation Energy in Rock Blasting. Geotechn Geolog Eng, 2008, 26(2): 133–146
17 Chen S Y, Liu L Q, Liu P X, et al. Theoretical and experimental study on relationship between strees-strain and temperature variation (in Chinese). Sci China Ser D-Earth Sci, 2009: 1446–1455
18 Xie H P, Ju Y, Li L Y. Criteria for strength and structural failure of rocks based on energy dissipation and energy release principles (in Chinese). Chin J Rock Mech Eng, 2005, 24(17): 3003–3010
19 Xie H P, Ju Y, Li L Y, et al. Energy mechanism of deformation and failure of rock masses (in Chinese). Chin J Rock Mech Eng, 2008, 27(9): 1729–1739
20 Gao H, Zheng Y R, Feng X T. Study on energy yield criterion of geomaterials (in Chinese). Chin J Rock Mech Eng, 2007, 26(12): 2437–2443
21 Peng R D, Xie H P, Ju Y. Analysis of energy dissipation and damage evolution of sandstone during tensile process (in Chinese). Chin J Rock Mech Eng, 2007, 26: 2526–2531
22 Peng R D, Ju Y, Xie H P. Fractal characterization of meso-structural evolution during tension of limestone (in Chinese). Rock Soil Mech, 2007, 28(12): 2579–2582
23 Xia C J, Ju Y, Xie H P. Numerical analysis of damage and energy dissipation in rock under blast loading (in Chinese). J Ballist, 2006, 18(3): 1–4
24 Li L Y, Ju Y, Zhao Z W. Energy analysis of rock structure under static and dynamic loading conditions (in Chinese). J China Coal Society, 2009, 34(6): 737–740
25 Yu Y, Yin J M. Energy dissipation properties of Three Gorges granite under different loading modes (in Chinese). Chin J Rock Mech Eng, 2004, 23(2): 205–208
26 Wang Q, Wang T, Yu C B, et al. Experimental research on dynamic modulus of elasticity and breaking absorbed energy of cement rock by SHPB (in Chinese). Earthquake Eng Eng Vibration, 2006, 26: 92–95
27 Lu J F. Energy dissipation mechanism research of rock deformation and failure process (in Chinese). Dissertation of Master Degree. Beijing: China University of Mining and Technology, 2009
28 Xia Z G. Plastic Mechanics (in Chinese). Shanghai: Tongji University Press, 1991
29 Yu M H. Unified Strength Theory and Its Applications. Berlin: Springer, 2004